*Journal of Ceramic Processing Research. Vol. 14, No. 1, pp. 96~99 (2013)*

J O U R N A L O F
**Ceramic Processing Research**

# Preparation and characterization of whitlockite-merwinite nanocomposite

**Masoud Hafezi[a,*], Marziyeh Abbasi-shahni[b], Ali Zamanian[a] and Saeed Hesaraki[a]**
[a]*Biomaterials Group, Nanotechnology & Advanced Materials, Materials and Energy Research Center, Iran*
[b]*Pardis Pajoohesh Fanavaran Yazd, BT center, Yazd Science and Technology Park, Yazd, Iran*

**The aim of this study is to investigate the properties of a novel nanocomposite made from whitlockite and nanostructured merwinite. In addition, the effect of merwinite on the apatite formation in this type of composite was evaluated. The nanostructured merwinite was successfully synthesized by the sol gel method. The synthesized merwinite was investigated by XRD and TEM. The nanocompositses were evaluated by SEM, FTIR before and after immersion in SBF. The apatite formation ability of the nanocomposites improved with an increase in the content of merwinite. Furthermore, SaSo-2 cells adhered and spread well on the nanocomposite. The results obtained in this experiment suggest that a whitlockite-merwinite nanocomposite could be a suitable choice for bone tissue engineering.**

**Key words: Biomaterial, Bioceramic, Nanocomposite, Merwinite, Whitlockite.**

## Introduction

For tissue engineering applications, many bioabsorbable composites, porous or non-porous have been used. A key factor for bone tissue engineering is utilizing absorbable biomaterials in manufacturing scaffolds in order to develop the growth of tissues [1]. Recently, different biopolymers, bioceramics and their biocomposites have been fabricated for bone tissue engineering [1-4].

Some of the calcium phosphate ceramics are resorbable. The calcium to phosphorus (Ca:P) atomic ratio in calcium phosphate minerals can be varied between 1.5 to 2. Tricalcium phosphate (TCP:$Ca_3(PO_4)_2$) is characterized by a Ca:P atomic ratio of 1.5 and is resorbable. However, controlling its bioresorbability is not easy [4]. TCP is available in two crystallographically different forms, α-TCP and β-TCP. The crystallographic form of β-TCP is often called whitlockite. β-TCP is less soluble in water than α-TCP [2]. The bioresorption of β-TCP typically takes place in a time period of 1-2 years [2]. All calcium phosphate ceramics such as TCP that have a high bioresorption rate have also been shown to exhibit large surface areas. Additionally, it is assumed that large surface areas can absorb endogenous proteins such as growth factors, from adjacent tissues which indicates that they can theoretically be indirectly osteoinductive and could therefore be considered to be even used as materials for tissue engineering [2].

The chemical composition is an important factor that affects the properties of materials. Previous reports have revealed that CaO and $SiO_2$ are common for the formation of bone-like apatite on the surface of some bioceramics after soaking in simulated body fluid (SBF) [5-10]. Pure $CaSiO_3$ powders and ceramics are highly bioactive and this feature makes them able to form a hydroxyapatite (HAp) layer on their surface after soaking in simulated body fluid (SBF) [11-12]. In order to form chemical bonds between bone and bioactive ceramics, this type of hydroxyapatite layer is mandatory [13]. Magnesium silicate ceramics have been reported as biocompatible bioceramics but their degradation rate and the apatite formation ability were poor [14, 15]. Excellent bioactivity of some calcium magnesium silicate ceramics such as akermanite, diopside and merwinite has been observed in SBF [8-10]. The ionic products from merwinite can stimulate osteoblast proliferation [8]. Consequently, the substitution of a directly bioactive material such as merwinite for the resorbable component might be done to achieve novel bioactive materials for bone tissue engineering.

In this study, merwinite-whitlockite nanocomposites with varied ratios were prepared which may provide an insight into the design of new composite ceramics with improved properties for bone tissue engineering.

## Material and Methods

### Beta tricalcium phosphate

Beta tricalcium phosphate (β-TCP) was synthesized by a solid state reaction from a stoichiometric mixture of calcium hydrogen phosphate anhydrous ($CaHPO_4$) [Merck], and calcium carbonate ($CaCO_3$) [Fluka] with a 2:1 molar ratio. the mixture of $CaHPO_4$ and $CaCO_3$ was heated in a platinum crucible at 950 °C for 3 h. After that the material obtained was ground and characterized by XRD.

*Corresponding author:
Tel : +98-26 36280040-9
Fax: +98-26 36201888
E-mail: mhafezi@merc.ac.ir

**Merwinite**

Merwinite was obtained by a sol-gel method reaction, starting from an appropriate mixture of ($Mg(No_3)_2 \cdot 6H_2O$) [Scharlau], ($Ca(NO_3)_2 \cdot 4H_2O$) [Merck], ($C_8H_{20}O_4Si$) [Merck] and ($HNO_3$) 0.1 M [Merck]. The starting sol was prepared by hydrolysis of tetra ethyl orthosilicate (TEOS) under magnetic stirring in the presence of 0.1 M $HNO_3$ solution for 60 minutes while the molar ratio of ($HNO_3 + H_2O$)/TEOS was fixed (TEOS:$HNO_3$:$H_2O$ = 1:4:16). Subsequently, solutions of $Mg(NO_3)_2 \cdot 6H_2O$ and $Ca(NO_3)_2 \cdot 4H_2O$ were added to the mixture (molar ratio: TEOS:$Mg(NO_3)_2.6H_2O$:$Ca(NO_3)_2 \cdot 6H_2O$ = 2:1:3). The sol was continuously and slowly stirred for 5 h and then kept at 60 °C overnight to allow gel formation. After 2 days, the resultant translucent gel was dried at 120 °C. The dried gel was heated for 24 h in an electrical box furnace at 700 °C using a heating rate 5 $Kminute^{-1}$ to eliminate residual nitrates.

**Merwinite-β-TCP samples**

The starting materials were synthesized β-TCP and merwinite. The desired proportions, given in Table 1, were weighed out and thoroughly mixed in a fast mill, then they were isostatically pressed into bars at 200 MPa. Samples were heated up to 1300 °C where they were held for 4 h. From this temperature the samples were cooled inside the furnace down to room temperature by shutting off the current.

**Sample characterization**

In order to identify the crystalline phases and to establish their compositions, the β-TCP and merwinite powders were characterized by an X-ray diffractometer (XRD; Philips PW 3710). Transmission electron microscopy (TEM; EM208S) and Fourier transform infrared spectroscopy (FTIR, Thermo Nicolet spectrometer) and a scanning electron microscope (SEM; Philips XL 30). As X-ray diffraction is sensitive to the crystallite size, the Scherrer formula [16] was used to determine the crystallite size of each material. The crystallite size of merwinite powder was determined using the Scherrer equation:

$$B = k\lambda/t\cos\theta \quad (1)$$

where λ is the wavelength (0.15406 nm), θ is the Bragg angle, k is a constant (0.9), and t is the apparent crystallite size. Structural changes were studied by FTIR. The FTIR spectra were recorded between 400 and 1400 $cm^{-1}$. The pellets were prepared by mixing each sample powder with a KBr matrix at a level of 1 wt.%. Background data was collected for the KBr matrix and subtracted from each spectrum.

Composite samples were immersed in SBF at 37 °C for 28 days to evaluate the in vitro bioactivity of samples.

**Table 1.** Powder composition (wt%) for preparing nanocomposite samples.

| | Composition (wt%) | | |
|---|---|---|---|
| | M2T8 | M4T6 | M6T4 |
| Merwinite | 20 | 40 | 60 |
| Whitlockite | 80 | 60 | 40 |

M and T refer to Merwinite and Whitlockite, respectively.

**Preparation of SBF**

SBF solution was prepared by dissolving reagent-grade NaCl, KCl, $NaHCO_3$, $MgCl_2 \cdot 6H_2O$, $CaCl_2$ and $KH_2PO_4$ in distilled water and buffered at pH = 7.25 with TRIS (Trimethylolaminomethane) and HCl 1M at 37 °C.

**Cell culture**

SaSo-2 osteoblast cells were used for biocompatibility tests. The cells were cultured in polystyrene plates enriched with Dulbecco's modified eagle medium (DMEM), (Gibco BRL), supplemented with 10% fetal bovine serum, 100 IU/ml penicillin (Sigma) and 100 mg/ml streptomycin (Sigma), and incubated at 37 °C in a humid atmosphere with 5%. When the cells reached confluence, the culture media was replaced by a media containing DMEM and nanostructured merwinite-whitlockite extracts and incubated for 72 h under the same conditions. Negative (ultra high molecular weight poly ethylene) and positive (copper) controls were used. After 72 h, the cells were observed under an optical microscope (Olympus IX71).

**SaSo-2 adhesion and morphology**

The SaSo-2 cells ($1.0*10^6$) were seeded on the nanocomposite ($5*5*10\ mm^3$) in a 48-well plate and incubated for 1 day in the DMEM culture medium supplemented with 15% fetal calf serum (FCS) maintained at 37 °C in a humidied atmosphere of 95% air and 5% $CO_2$. After different culture times, the scaffolds were removed from the culture wells and rinsed with phosphate buffered saline (PBS). For SEM observation, the cells on scaffolds were fixed with 2.5% glutaraldehyde, dehydrated in a grade a ethanol series (30, 50, 70, 90, and 96%(v/v)) for 10 minutes, with a final dehydration in absolute ethanol twice followed by drying in hexamethyldisilizane (HMDS) ethanol solution series.

## Results and discussions

Fig. 1 shows the X-ray diffraction patterns of the synthesized powder of β-TCP and merwinite. It can be seen that the polymorphic forms obtained are β-TCP and merwinite corresponding to JCPDS card no. (009-169) and (01-074-0382), respectively [14]. The crystallite sizes of merwinite and β-TCP phases were calculated by the Scherrer equation. The synthesized merwinite at 700 °C and β-TCP at 950 °C show crystallite size of approximately 35 nm and 52 nm, respectively.

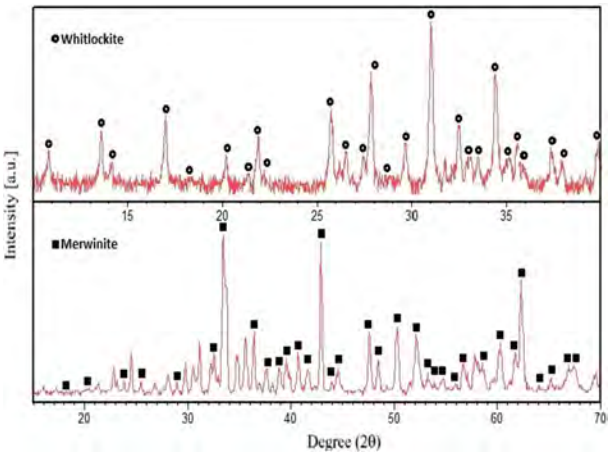


**Fig. 1.** X-ray diffraction patterns of the synthesized powder.

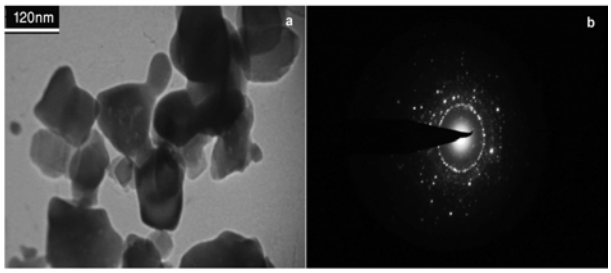


**Fig. 2.** TEM micrograph(a) and electron diffraction pattern(b) of merwinite particles.

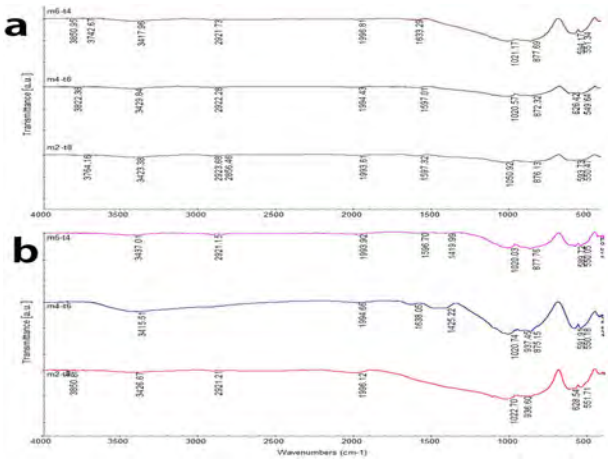


**Fig. 3.** FTIR spectra of the nanocomposite samples after soaking in SBF for (a) 1 and (b) 28 days.

A TEM micrograph and diffraction pattern for merwinite are shown in Figure 2. It is obvious that the crystallites of merwinite powder exhibit agglomerated morphologies with pretty spherical shapes. The crystallite size of the merwinite powder obtained was in the range of 30-70 nm with a mean value of about 40 nm.

As figure 3 shows all FTIR spectra present similarities. A band shows at 1050-1020-1021 $cm^{-1}$ due to the Si-O-Si stretching vibrations, indicating the presence of silicate groups. Bands around 400, (593-626-594) and (3423-3429-3417) $cm^{-1}$, are attributed to

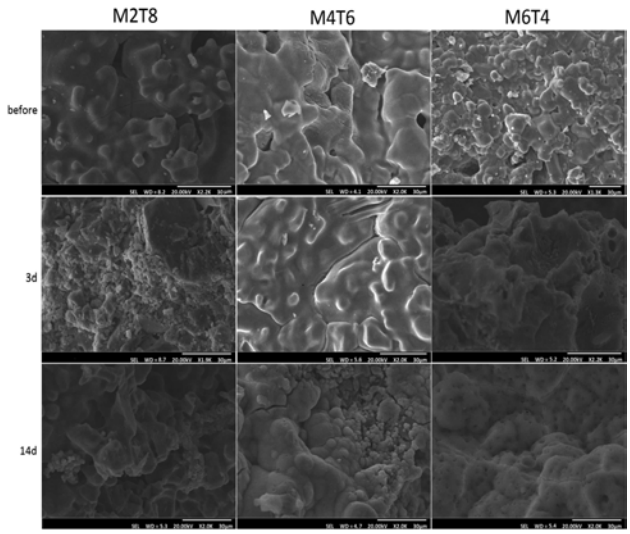


**Fig. 4.** SEM micrographs of the nanocomposites samples before and after 3 and 14 days soaking in SBF.

Mg-O, Ca-O and apatite O-H, respectively. Bands between 1590-1630 $cm^{-1}$ are related to δHOH. The bands in the (550-549-551) $cm^{-1}$ are assigned to a the components of the asymmetric P-O stretching mode ($\nu_4$). Additional characteristics from the Carbonated Hap layer are one or two weak bands at (1597-1597) $cm^{-1}$ assigned to C-O stretching vibration and one at (876-872-877) $cm^{-1}$ assigned to a C-O out-of-plane bending vibration of the carbonate group [10, 17-18].

Unfortunately, because the $SiO_4^{4-}$ tetrahedra vibrations overlap with the same type of vibrations in the $PO_4^{3-}$ tetrahedra, the main bands corresponding to the silicate group cannot be distinguished.

The phosphate peaks became more intense and sharper with an increase in the immersion time, indicating the growth of crystalline apatite in vitro. These results suggest that the apatite formed on the surface of specimens in SBF is carbonated apatite, which is similar in composition and structure to bone apatite [10, 17].

SEM micrographs of the nanocomposite samples before and after 3 and 14 days soaking in SBF are shown in figure 4. Image of the surface of the dense composites sintered at 1300 °C are shown in the figure 4. Fine precipitates were observed on the surfaces of samples after soaking in SBF within 14 days. SEM micrographs of the M6T4 sample show degradation caused a porous structure after 14 days. One possible alternative could be the degradation of merwinite in physiological conditions. Previous results indicated that Mg contents in the $CaO\text{-}MgO\text{-}SiO_2$ system, have an important role in degradability of this type of ceramic [18]. In addition, the crystallographic structure of merwinite affects its degradability [18-19]. However further studies are required to determine the relationship between the compound and the crystallographic structure of this ceramic.

An optical microscope image of the SaSo-2 osteoblast

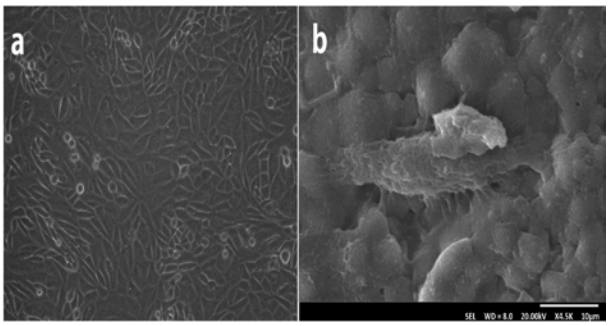


**Fig. 5.** a) Optical microscope image of the SaSo-2 osteoblast cells after an incubation period of 72 h and b) SEM micrograph of merwinite-whitlockite nanocomposite after culturing for 24 h.

cells after an incubation period of 72 h and a SEM micrograph of the merwinite-whitlockite nanocomposite after culturing for 24 h are shown in figure 5. The cells displayed a spindle-shaped morphology and formed a monolayer. It was obvious that SaSo-2 adhered and grew on the nanocomposite surface.

The Surface morphology and chemical composition of the biomaterial were responsible for its cellular response [20-21]. It has been reported in previous studies that dissolving Si and Mg ions from a bioactive glass could stimulate the proliferation and adhesion of osteoblastic cells [22-24]. Mg ions also affect bone remodeling [23]. It is confirmed that Ca and Si ions play a critical role in the process of nucleation and growth of hydroxyapatite. They affect the mineralization process and bone-bonding mechanism [25]. We believe that the release of Ca, Mg, and Si from the merwinite bioceramic plays an important role in the adhesion and proliferation of cells and the formation of apatite which might be attributed to the release of substances containing Ca, Mg, and Si from the merwinite bioceramic although we cannot absolutely rule out the influence of the microstructure on the cell behavior. The detailed mechanism needs further investigations.

## Conclusions

In summary merwinite and whitlockite powders were synthesized by the sol-gel and solid-state reaction methods, respectively. Sintered merwinite-whitlockite nanocomposites have the ability to form a bone-like apatite after soaking in SBF. The apatite formation ability was improved by increasing the merwinite in the composites. Furthermore, osteoblasts spread well on the surface of merwinite-whitlockite nanocomposites. They can be a suitable candidate for bone replacement. However, further in vitro and in vivo studies are required to explore the applicability of these composites as implant materials.

## Acknowledgment

The authors would like to acknowledge the Iran National Science Foundation (INSF) for the financial support of this work, through grant No. 90007188.

## References

1. M. Wang, L.J. Chen, J. Ni, J. Weng and C.Y. Yue, J. Mater. Sci. Mater. Med. 12 (2001) 855-860.
2. G. Grandi., C. Heitz, L.A.D. Santos, M.L. Silva, M.S. Filho, R.M. Pagnocelli and D.N. Silva, J. Mater. Res. 14 (1) (2011) 11-16.
3. W. Paul, C.P. Sharma, J. Biomater. Appl. 17 (4) (2003) 253-264.
4. M. Kamitakahara, C. Ohtsuki, Y. Kozaka, S. Ogata, M. Tanihara, and T. Miyazaki. J. Ceram. Soc. Jpn. 114 (1325) (2006) 82-86.
5. A. Merrolli, P.T. Leali and P.L. Guidi. J. Mater. Sci. Mater. Med. 11 (2000) 219-222.
6. K.H. Karlsson, Glass Technol. 45 (2004) 157-161.
7. S. Agathopoulosa, D.U. Tulyaganova, J.M.G. Ventura, S. Kannana, M.A. Karakassides and J.M.F. Ferreira, J. Biomaterials. 27 (9) (2006) 1832-1840.
8. M. Hafezi-Ardakani, F. Moztarzadeh, M. Rabiee, A.R. Talebi, M. Abasi-shahni, F. Fesahat and F. Sadeghian, J. Ceram. Process. Res. (2010) 11765-11768.
9. V.B. Bhatkar and N.V. Bhatkar, IJAEST. 5 (2) (2011) 184 - 186.
10. M. Hafezi-Ardakani, F. Moztarzadeh, M. Rabiee, A.R Talebi, J. Ceram. Int. 37 (2011) 175-180.
11. P. Siriphannon, Y. Kameshima, A. Yasumori, K. Okada and S. Hayashi, J. Biomed. Mater. Res. 52 (2000) 30-39.
12. P. Siriphannon, Y. Kameshima, A. Yasumori, K. Okada and S. Hayashi, J. Eur. Ceram. Soc. 22 (2002) 511-520.
13. K. Lin, Z. Wanyin, S. Ni, J. Chang, Y. Zeng and W. Qian, J. Ceram. Int. 31 (2005) 323-326.
14. M. Abbasi-Shahni, S. Hesaraki, A.A. Behnam-Ghader and M. Hafezi-Ardakani, J Key Eng. Mater. 493-494 (2011) 582-587.
15. S.Y. Ni, L. Chou, J. Chang, J. Ceram. Int., 33 (2007) 83-88.
16. H. Klug, L. Alexander, in X-Ray diffraction procedures, Wiley Press (1962).
17. C. Wu and J. Chang,, J. Biomed. Mater. Res., Part B. 83 [1] (2007) 153-156.
18. K.P. Sanosh, A. Balakrishnana, b, L. Francisc and T.N. Kima, J. ALLOY COMPD, 495 (2010) 113-115.
19. S.R. Radin, P. Ducheyne J Biomed Mater Res 28 (1994) 1303-1309.
20. U. Meyer, A. Büchter, H.P. Wiesmann, U. Joos, D.B. Jones J. Eur Cell Mater 26 (2005) 39-49.
21. A. Hoppe, N.S. Güldal, A.R. Boccaccini, J. Biomaterials 32 (2011) 2757-2774.
22. J.E. Gough, J.R. Jones, L.L. Hench, J. Biomaterials 25 (2004) 2039-2046.
23. J.W. Park, Y.J. Kim, J.H. Jang, H.Song J. Clin Oral Implants Res 21 (2010) 1278-1287.
24. E. Abed, R. Moreau, J. Cell Prolif 40 (2007) 849-865.
25. D. Dufrane, C. Delloye, I.J. McKay, P.N. De Aza, S. De Aza, Y.J. Schneider, M.Anseau J. Mater Sci Mater Med 14 (2003) 33-38.